Effects of Temperature and Light Illumination on the Current– Voltage Characteristics of Molecular Self-Assembled Monolayer Junctions

ARTICLE *in* THE JOURNAL OF PHYSICAL CHEMISTRY C · MAY 2012

Impact Factor: 4.77 · DOI: 10.1021/jp300467c

3 AUTHORS, INCLUDING:

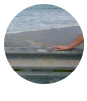

Dechun Ba
Northeastern University (Shenyang, China)
30 PUBLICATIONS **44** CITATIONS

THE JOURNAL OF PHYSICAL CHEMISTRY C

Article

pubs.acs.org/JPCC

Effects of Temperature and Light Illumination on the Current−Voltage Characteristics of Molecular Self-Assembled Monolayer Junctions

Jian-Chang Li,* Dan Wang, and De-Chun Ba

Vacuum and Fluid Engineering Research Center, Northeastern University, Shenyang 1100819, People's Republic of China

Supporting Information

ABSTRACT: We systematically studied the charge transport properties of a series of self-assembled monolayer crossbar junctions with different alkanethiol and conjugated molecules, respectively. The junction was fabricated using a soft stamp-printing method. Current−voltage characteristics were measured at varied temperatures between 300 down to 90 K under different light illumination conditions. Strong temperature dependence and optoelectronic switching phenomena were observed in the as-fabricated junctions in both dark and light situations. To understand the charge transport mechanism, the Simmons and Fowler−Nordheim tunneling were used to analyze the experimental data. The distinctly different adsorbing nature of the top printed Au/molecule interface in the crossbar junctions is shown to play a dominant role in causing the asymmetric transport behavior. The charge injection barrier is strongly dependent on both the substrate temperature and the molecular length/conjugation structures. The barrier decreases with the increase of the substrate temperature and/or the molecular length, while a conjugated molecular structure can obviously enhance the junction charge transport. Our work may offer some useful information for developing molecular electronic devices.

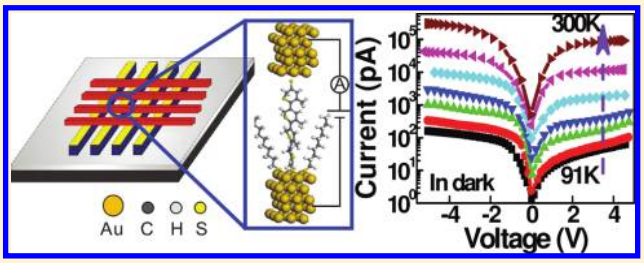

INTRODUCTION

Molecular electronics is a fascinating scientific frontier and an interdisciplinary research topic with potential applications in a variety of technological fields.[1,2] Unlike inorganics such as diamond, silicon, and germanium,[3−5] organic thin films have advantages in flexibility, low-cost, easy processing, and controllable molecular design,[6] which are wildly studied for use in light-emitting diodes,[7] thin film transistors,[8] and solar cells.[9]

Self-assembled monolayers (SAMs) are ordered, functionalized molecular assemblies that form spontaneously by adsorption of an active surfactant with a specific affinity of its headgroup to an appropriate substrate.[10] Alkanethiols and conjugated molecules are the most common SAMs materials,[11−16] which can with relative ease grow uniform, densely packed, and large area monolayers. For example, the SAMs of a series of alkanethiols were studied by using conducting atomic force microscopy (C-AFM) to investigate the molecular length dependence of the low-bias conductance, the transition voltages, and the tunneling attenuation factors.[17−19] Oligothiophene has a low band gap and can be easily derivatized into some covalent architecture. The solution and solid-state aggregation of oligothiophenes have been well-characterized for use in optoelectronic devices.[20]

Molecular charge transport is influenced by various factors including molecular structure, metal−molecule interface(s), light illumination, and temperature, and so forth.[21−23] Greater understanding of the charge transport may open new possibilities for engineered molecular devices. Especially, as one of the most powerful test-beds, the metal−molecule−metal junction is of great use.[24,25] For example, Kaun et al. studied the alkanethiol SAMs with different lengths and found that the transport is largely determined by the molecule itself.[26,27] Wang et al. investigated the influence of molecular configuration on the electrical properties of alkyl and conjugated junctions. They show the intramolecular conformation and intermolecular interaction can both affect the junction charge transport.[21,28] Beebe et al. indicated the contact resistance in molecular junctions is affected significantly by the metal/molecule interface(s).[22] Effects of light illumination and temperature were also shown to be important factors influencing the charge transport.[29,30]

In this article, we fabricated addressable molecular crossbar junctions using a polymer stamp-printing approach. The charge transport of a series of molecular junctions with different alkanethiol and conjugated SAMs was systematically investigated through current−voltage (I−V) measurements at varied low temperatures and under different illumination conditions. The I−V characteristics were analyzed and simulated, indicating that the charge injection barrier across the molecular junctions is strongly dependent on the substrate temperature, light illumination, metal/molecule interfaces, and molecular length/conjugation. The charge transport mechanism is tentatively discussed.

Received: January 15, 2012
Revised: May 3, 2012
Published: May 7, 2012

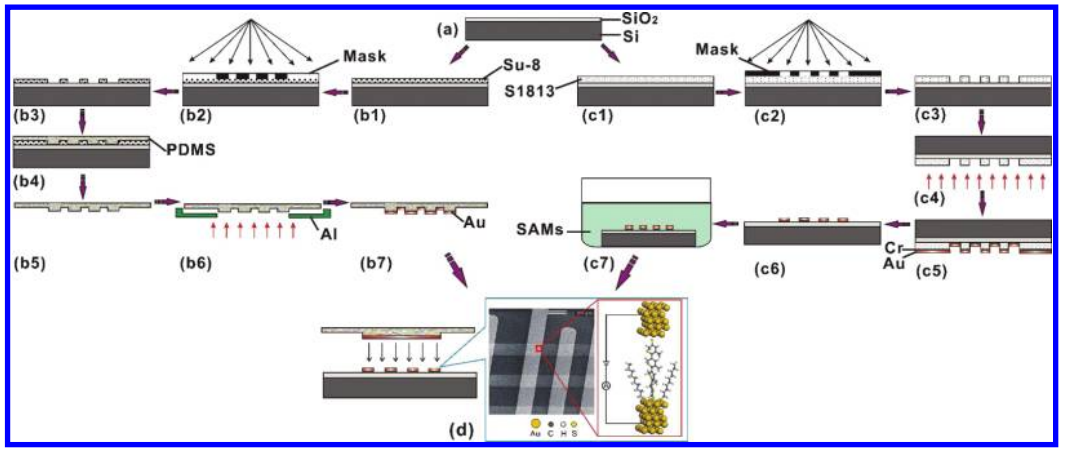

Figure 1. Schematic drawings show how the crossbar junctions are fabricated. (a) Clean Si(100) substrate grown with 250-nm-thick SiO_2 on double sides. The preparation of the upper electrodes includes: (b1) spin-coating negative photoresist, (b2) exposure under predesigned mask, (b3) hard-baking, (b4–b5) PDMS stamp fabrication via casting and curing the prepolymer against the mold, (b6–b7) depositing Au onto the stamp, respectively. The preparation of the bottom electrodes includes: (c1) spin-coating positive photoresist, (c2) exposure under predesigned mask, (c3) hard-baking, (c4–c5) depositing Cr and Au, (c6) clean up the positive photoresist, (c7) generation of the SAMs. (d) Stamp-printing and the as-fabricated crossbar junctions with its structure schematically shown.

EXPERIMENTAL SECTION

A soft polymer stamp-printing method is used to fabricate the addressable molecular crossbar junctions, which provides a simple way to obtain optoelectronic switches and transistors driven by a low frequency alternating current (AC) electrical field.[31] Figure 1 shows how the junctions are prepared. The Si (100) substrate with 250-nm-thick SiO_2 on both sides was first cleaned in a hot "piranha solution" (a 4:1, v/v, mixture of concentrated H_2SO_4 and 30% H_2O_2) for 10 min (Figure 1a). It is followed by thorough rinsing with deionized water, acetone, and ethanol, respectively. The bottom electrode patterns (50 nm thick) are then fabricated by conventional photolithography and thermal vapor deposition (Figure 1c1–c6) with the experimental parameters given in Table 1.

Table 1. Experimental Parameters for Fabrication of the PDMS Stamp-Printing Crossbar Junctions

process	for Au bottom electrode	for PDMS mold
photoresist	positive resist S1813	negative resist SU-8
spin-coat	3.5 krpm, 60 s	3 krpm, 80 s
soft-bake	115 °C, 60 s	65 °C, 120 s → 95 °C, 300 s
cooling	180 s	180 s
exposure	60 s	85 s
hard-bake	115 °C, 180 s	65 °C, 60 s → 95 °C, 120 s
cooling	180 s	180 s
develop	45 s	90 s
vacuum vapor deposition	Cr, 7.5 nm; Au, 50 nm	Au, 20 nm
deposition rate	0.3 nm/s	1 nm/s
clean	thoroughly rinse with acetone and deionized water flow and blow-dry with nitrogen gas	

The target molecular SAMs are made by immersing the as-fabricated electrode patterns in 1 mM molecular solution in pure tetrahydrofuran (THF) for 24 h (Figure 1c7). The SAMs growth is controlled through a sequential deprotection and immobilization procedures as formerly described.[32] Briefly, the cyanoethyl protecting group is cleaved in situ with sodium ethoxide to form a free thiol ending group. Then, the molecules are self-assembled onto the gold electrode. Last, the trimethylsilylethyl protecting group on top of the SAMs is cleaved with a solution of tetrabutylammonium fluoride in THF.[33]

An elastomeric poly(dimethylsiloxane) (PDMS) stamp is used to print the top Au electrode bars. As shown in Figure 1b1–b5, the stamp is prepared by casting and curing the prepolymer against a SU-8 negative photoresist mold. A 20-nm-thick Au layer is vapor deposited onto the stamp cooled by liquid nitrogen (see Figure 1b6,b7). Under microscope, the stamp is then brought into perpendicular contact with the prefabricated substrate/Au bars with SAMs at room temperature (Figure 1d). The substrate/stamp set is then placed into a vacuum chamber and cooled down to 95 K for 10 min. After warming up, the stamp is carefully removed so that the top Au electrodes are transferred onto the substrate. An overall good junction rate of 15% is achieved. On an average, for each molecule studied, at least 10 good junctions are measured on different substrates.

The sample is loaded into a vacuum chamber where low-frequency (0.002 Hz) AC $I-V$ characteristics are measured using a HP 3325A synthesizer/function generator and a Keithley 619 electrometer with bias scanning range of ±5 V and at varied low temperatures (90–300 K) with or without light illumination. As in the design of conventional microelectronics, the local heating effect due to the high current densities is another important factor affecting the metal–molecule–metal junction transport.[34−36] In our case, the $I-V$ measurements are mostly carried out at a low temperature with a relatively large junction area (~900 μm^2). The device current density is thus much smaller than that of the scanning probe microscope-based junctions. To simplify the problem, local current-induced heating effects are neglected in the following discussions.

Figure 2 shows the chemical structure of the molecules studied, which are carefully selected to investigate the effects of molecular length, ending substituent groups, and conjugation degree on the junction charge transport, respectively. Here, 1-octanethiol (OT), 1-decanethiol (DT), 1,9-nonanedithiol (NDT), and 1-dodecanethiol (DDT) stand for saturated

dx.doi.org/10.1021/jp300467c | J. Phys. Chem. C 2012, 116, 10986–10994

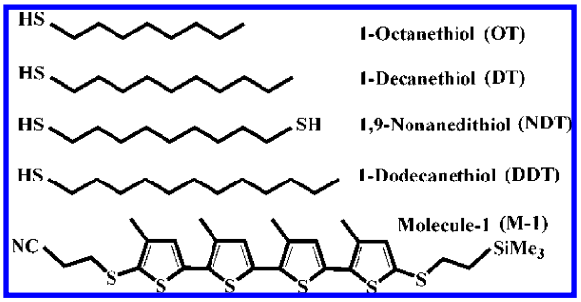

Figure 2. Chemical structure of the alkanethiols and conjugated molecule studied with different molecular lengths, ending substituent group, and/or conjugation degree, respectively.

alkanethiols and a kind of oligothiophene named as molecule-1 (M-1) represents for conjugated materials.

RESULTS

Conduction Mechanisms. The possible conduction models are summarized in Table 2 with the dependences of temperature and voltage highlighted. The mechanisms fall into two distinct categories based on whether thermal activation is involved or not. The direct tunneling and the Fowler–Nordheim (F–N) transport are independent of temperature, while the hopping conduction, the Poole–Frenkel (P–F), and the thermionic emission are all temperature-dependent. For example, the direct tunneling and F–N are used to study the charge transport across molecular junctions of alkanethiols and oligo(phenylene ethynylene).[2,37,38] Hopping conduction, P–F, and thermionic emissions have been observed for junctions of conjugated heterocyclic oligomers,[39] 1,4-phenylene diisocyanide,[40] and conjugated organic dye molecular SAMs,[41] respectively.

I–V characteristics provide important insight into the junction charge transport. Without temperature-dependent measurements, it is difficult to assign the transport mechanism.[42] As shown in Figure 3a,b, we carried out I–V characterization for the DT junctions at temperatures of 300 K down to 90 K. Strong temperature dependence was observed from the asymmetric curves. For instance, the current ratios between 300 and 91 K are about 10^3 and 10^1 at ±1 V under light illumination, respectively. A similar phenomenon also exists in the dark conditions but with current ratio of about 10^3 at ±1 V between 300 and 91 K, respectively. Note that the junction shows entirely different behaviors in the dark and light situations. Unlike the previous report,[43] it seems that the alkanethiol SAMs may have temperature dependence in some cases. This may be caused by the different electronic nature of the Au/molecule interface(s) in our stamp printed crossbar junctions. The printing approach may influence the metal/molecule interfacial structure to some extent, which further affects the charge injection and transport across the junction.[44,45]

According to the direct tunneling, the I–V data of the DT junction were plotted on a linear scale in Figure 4a,b. The plots of I vs V show preferable linear relation in both dark and light conditions at conditions of low temperature (91–185 K) and low bias (−1 to +1 V), suggesting the direct tunneling plays a dominating role. The plots of $\ln(I/V^2)$ vs $1/V$ are linear and nonlinear under dark and light conditions, respectively (see Figure 4c,d). Therefore, the F–N tunneling may act as the transport mechanism only in the dark situation. Further studies of the I–V temperature dependence indicate that the junction transport obeys no mechanisms of the hopping conduction, P–F model, and thermionic emission. Therefore the overall analysis suggests that the direct tunneling plays a dominant role at −1 to +1 V under both dark and light illumination, while the F–N tunneling is applicable at high bias range only under dark situations.

Simmons Model. To analyze the junction charge transport, the I–V curves were fitted by the Simmons model, which is the simplest one for electron tunneling through metal–insulator–metal systems. The Simmons equation expresses the current through a rectangular barrier in the tunneling regime of $V < \Phi_{Sim}/e$ as:[46]

$$J = \frac{Ce}{4\pi^2\hbar d^2}\left\{\left(\Phi_{Sim} - \frac{eV}{2}\right)\exp\left[-\frac{2(2m)^{1/2}}{\hbar}\alpha\left(\Phi_{Sim} - \frac{eV}{2}\right)^{1/2}d\right] - \left(\Phi_{Sim} + \frac{eV}{2}\right)\exp\left[-\frac{2(2m)^{1/2}}{\hbar}\alpha\left(\Phi_{Sim} + \frac{eV}{2}\right)^{1/2}d\right]\right\} \quad (1)$$

where Φ_{Sim} is the barrier height, V is the applied bias, e is the charge of an electron, $\hbar = h/2\pi$ (h is Planck's constant), d is the tunneling distance, m is the mass of an electron, C is a proportionality constant, and α is a unitless adjustable parameter that is introduced to modify the simple rectangular barrier or to account for an effective mass in the fitting.[47,48] In this work, we discuss the current instead of current density.

Table 2. Summary of Feasible Conduction Mechanisms

conduction mechanisms	characteristic behavior	temperature dependence	voltage dependence
direct tunneling	$I = S\frac{q^2V\alpha}{\hbar^2 d}(2m\phi)^{1/2} \times \exp\left(\frac{-2\alpha d}{\hbar}(2m\phi)^{1/2}\right)$	none	$I \propto V$
Fowler–Nordheim tunneling	$I = \frac{Smq^3}{8\pi hm^*\phi_{FN}}E^2 \times \exp\left(-\frac{4\sqrt{2m^*}(\phi_{FN})^{3/2}}{3hqE}\right)$	none	$\ln(I/V^2) \propto 1/V$
hopping conduction	$I = \frac{S}{d}V\sigma_0 \exp\left(-\frac{E_a}{kT}\right)$	$\ln(I/V) \propto 1/T$	$I \propto V$
Poole–Frankel emmission	$I = SV \exp\left(-\frac{q(\phi_{PF} - \sqrt{qE/\pi\varepsilon\varepsilon_0})}{kT}\right)$	$\ln(I) \propto 1/T$	$\ln(I/V) \propto V^{1/2}$
thermionic emission	$I = SAT^2 \exp(e\beta E^{1/2} - \phi_0)/kT$	$\ln(I/T^2) \propto 1/T$	$\ln(I) \propto V^{1/2}$

dx.doi.org/10.1021/jp300467c | J. Phys. Chem. C 2012, 116, 10986–10994

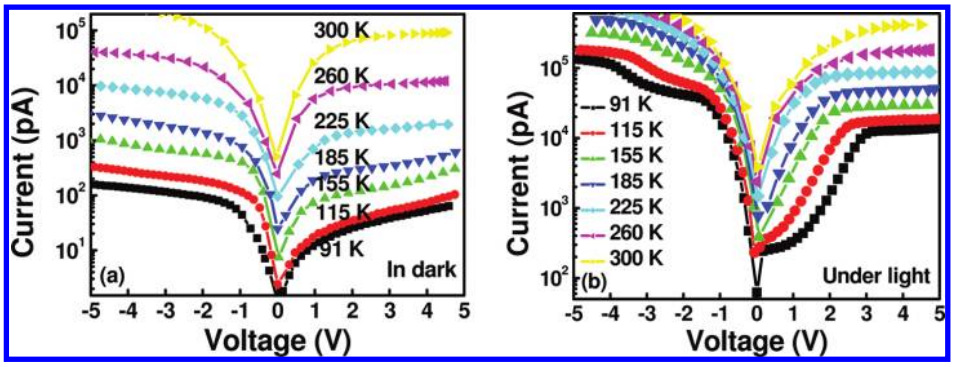

Figure 3. Typical $I-V$ characteristics of the DT crossbar junction measured from 91 up to 300 K (a) in the dark and (b) under light conditions, respectively.

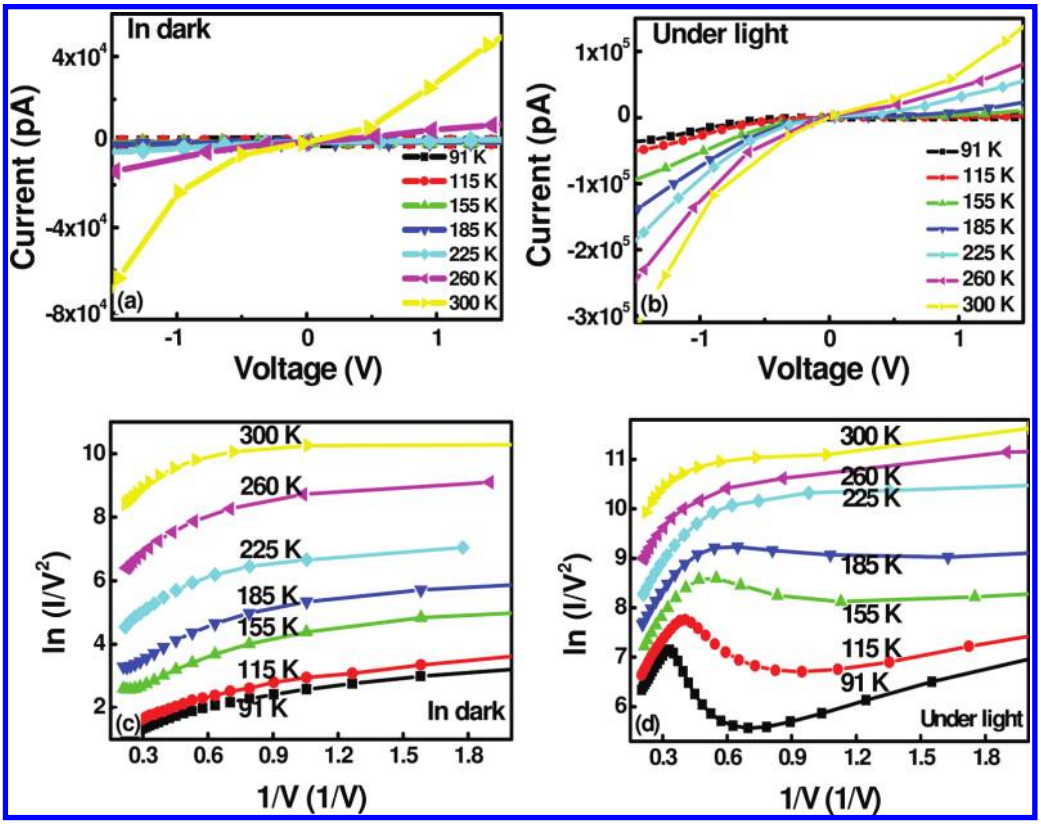

Figure 4. Typical $I-V$ curves of the DT junction on a linear scale (a) in the dark and (b) under light, respectively. Plots of $\ln(I^2/V)$ vs $1/V$ at different temperatures; (c) in the dark and (d) under light, respectively.

Thus, eq 1 is multiplied by S, which is the junction area. The Simmons model is only a crude approximation for electron tunneling in molecular junctions at a low bias range (normally within ±1 V),[42,49] and eq 1 can be thus approximated as the following form with three parameters of Φ, α, and C, respectively,

$$I = S\frac{C(2m\Phi_{Sim})^{1/2}e^2}{\hbar^2 d}\alpha V \times \exp\left[\frac{-2(2m)^{1/2}}{\hbar}\alpha(\Phi_{Sim})^{1/2}d\right] \quad (2)$$

where the current is exponentially dependent on the tunneling distance d. Thus, the exponential factor dominated in eq 2 can be regarded as $I \approx \exp(-\beta d)$ with

$$\beta = \frac{2(2m)^{1/2}}{\hbar}\alpha(\Phi_{Sim})^{1/2} \quad (3)$$

where β is a bias-independent but structure-dependent decay coefficient, which can be calculated by simulating Φ_{Sim} and α.

The experimental $I-V$ data is simulated using eq 2. Figure 5 presents a typical fit of the DT junction on a logarithmic scale in the positive low-bias region (0 to +1 V) at different temperatures in dark. It is indicated that, at low temperatures (91 to 185 K), the $I-V$ data satisfies the Simmons model quite well. The charge injection barrier heights are simulated to be about 1.50 and 1.39 eV at 91 and 300 K, respectively. Likewise, the $I-V$ curves are systematically fitted for other bias regions under both dark and light illumination. Figure 6 summarizes the fitting results for the DT junction. It is shown that in the dark the best fitting parameters are α = 0.65 and β = 0.81 ± 0.01 Å^{-1}, respectively. The Φ_{Sim} decreases by about 7% from 1.50 eV at 91 K to 1.39 eV at 300 K at positive bias, while the corresponding decrease is about 3% from 1.47 to 1.42 eV at the

dx.doi.org/10.1021/jp300467c | J. Phys. Chem. C 2012, 116, 10986−10994

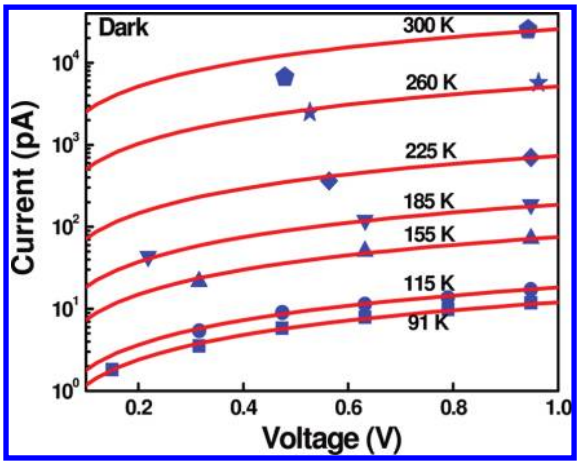

Figure 5. Simulation results for the DT junction in the dark condition. Experimental data (solid points) and the fitting curves (the lines) are ploted for different temperatures. Here, the best fitting parameters are α = 0.65 and β = 0.81 ± 0.01 Å^{-1}, respectively. The barrier heights used in the plots are 1.5, 1.49, 1.49, 1.46, 1.44, 1.43, and 1.39 eV for 91, 115, 155, 185, 225, 260, and 300 K, respectively.

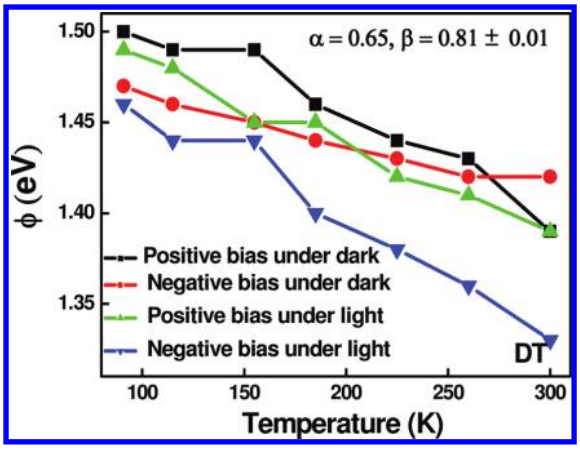

Figure 6. Best-fitting parameters obtained by the Simmons model for the DT junction at different conditions. The barrier height decreases with the increasing substrate temperature, which is higher at the positive voltage than that at the negative side because of the asymmetric electrode/molecule interfaces. The barrier height is higher in dark condition than that under light illumination.

negative bias, respectively. On the contrary, the values of α and β keep the same under light illumination. However, the Φ_{Sim} reduces by about 7% from 1.49 eV at 91 K to 1.39 eV at 300 K at the positive bias with the decrease of about 9% from 1.46 to 1.33 eV at the negative bias. These observations suggest that the barrier height is temperature-dependent in accordance with the previous report that the barrier falls off with the increase of temperature.[37]

The barrier height is also shown to be dependent on the bias direction with values larger at the positive side. This may be caused by the asymmetric interfaces of the two metal/molecule contacts of our crossbar junctions.[38] The top Au electrode was just softly stamp-printed onto the SAMs surface, while the molecules were anchored to the bottom electrode surface via a strong S−Au chemical bond. According to Seminario's analysis the S−Au physisorbed interface provides a particularly poor characteristic, which can be considered "insulating", for electron transport.[50] We thus treat the top SAMs-Au interface as a blocking layer for electron tunneling. Furthermore, the barrier height is found to be influenced by light illumination to some extent. As shown in Figure 3, the junction is more conductive under light because the light absorption may generate carrier-contributing photocurrent.[51]

We further simulated the fitting parameters for other molecules of OT, NDT, DDT, and M-1, respectively. It is shown that the values of α are the same for each kind of molecules at different conditions, while the barrier height Φ_{Sim} is different. Figure 7 plots the barrier heights for different

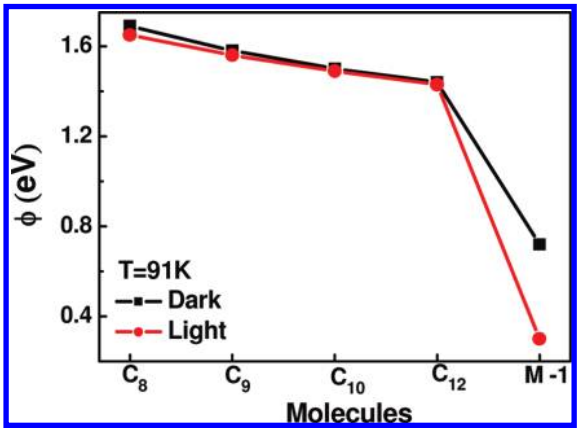

Figure 7. Plots of the Φ values obtained by the Simmons model for the molecules studied in the dark and under light conditions, respectively.

molecules in the positive bias at 91 K. The Φ_{Sim} of alkanethiols decreases with increasing molecular length from about 1.69 eV for OT down to approximately 1.44 eV for DDT under the dark condition, while the corresponding change is 1.65 to 1.42 eV under light illumination. On the other hand, the Φ_{Sim} of M-1 is about 0.72 and 0.3 eV under dark and light, respectively. The results suggest that the junction barrier height is a molecular length and conjugation-dependent parameter.[28,52] For example, Wang et al. observed a barrier height of 1.83 eV for OT down to 1.42 eV for DDT,[53] while David et al. reported that the tunneling-barrier height for oligo-p-phenylene is about 0.25 eV.[54]

The β values show a similar change trend decreasing from 0.86 ± 0.01 Å^{-1} for OT to 0.80 ± 0.01 Å^{-1} for DDT, respectively. For M-1 molecule, the value is 0.56 ± 0.06 Å^{-1} in the dark and 0.37 ± 0.02 Å^{-1} under light, respectively. The theoretical estimate presented herein is in reasonable agreement with previous literature observations.[19,55,56]

In Table 3, we summarized the parameters of Φ and β for different molecules measured using various approaches. It is shown that, with different test methods and/or device structures, the as-obtained barrier height for the same molecular material varies tremendously. For example, the Φ of DDT is 1.42 and 2.2 eV measured by C-AFM and scanning tunneling microscopy (STM), respectively.[27,57] The Φ of ODT is 1.69 and 1.83 eV in STM/SAMs/Au and Au/SAMs/Au device structures, respectively.[47,48] The barrier height is largely dependent on molecular structure. For instance, Kitagawa et al. obtained 2.83, 2.76, and 2.17 eV for DDT, SL16B and SL16Fc, respectively,[46] whereas Seo et al., using the same model and device structure, got a barrier height of about 1.49 and 1.69 eV for OT and ODT, respectively.[48]

dx.doi.org/10.1021/jp300467c | J. Phys. Chem. C 2012, 116, 10986−10994

Table 3. Summary of the Values of ϕ, α, and β for Organic Molecules Obtained by Different Methods

molecular material	device structures	test method	model	ϕ (eV)	α	β (Å^{-1})	ref
OT	STM/SAMs/Au	STM	Simmons	1.49	0.8	1.0	48
OT	Au/SAMs/Au	CAFM	Simmons	1.83	0.61	0.85	27
DT	TTF/SAM/Au	AFM	Simmons	1.51	0.67	0.87	71
DDT	Au/SAMs/Au	CAFM	Simmons	1.42	0.65	0.79	27
DDT	Au/SAMs/Au	CP-AFM	Simmons	3.4	0.95	0.76	49
DDT	Au/SAMs/Au	CP-AFM		2.2		1.19	57
DDT	AFM/SAMs/Au	CP-AFM	Simmons	1.51	0.67	0.85	72
ODT	STM/SAMs/Au	STM	Simmons	1.69	0.76	1.02	48
ODT	Au/SAMs/Au	STM	Simmons	1.83	0.61	0.85	47
HDT	Ag/SAMs/Hg	AFM		2.1	0.62	0.87	56
HDT	Au/SAMs/Au	CAFM	Simmons	1.40	0.68	0.82	22
SL16B	STM/SAMs/Au	STM	Simmons	2.76	0.44	0.75	46
SL16Fc	STM/SAMs/Au	STM	Simmons	2.17	0.47		46

Fowler–Nordheim Model. Tunneling in the high-voltage regime is synonymous with tunneling through a triangular barrier and with the terms field emission and F–N tunneling.[38] Beebe et al. recently demonstrated that the I–V characteristics of oligo(phenylene ethynylene) junctions measured using crossed-wire and C-AFM exhibit a transition from direct tunneling to F–N tunneling, which occurs at biases ranging from 1.5 to 2.0 V.[18] It is shown that our experimental data can be fitted by the F–N model in a bias range of −2.5 to +2.5 V at high temperature region of 185–300 K. The F–N tunneling is expressed as[58]

$$J = AE^2 \exp\left(-\frac{B}{E}\right) \tag{4}$$

where E is the electrical field in the insulator. The pre-exponent A and the slope B are given by[59]

$$A = \frac{mq^3}{8\pi hm^*\phi_{FN}} \tag{5}$$

$$B = \frac{4\sqrt{2m^*}(\phi_{FN})^{3/2}}{3hq} \tag{6}$$

where Φ_{FN} is the barrier height. Equation 4 can be written as

$$I = \frac{Smq^3}{8\pi hm^*\phi_{FN}} E^2 \times \exp\left(-\frac{4\sqrt{2m^*}(\phi_{FN})^{3/2}}{3hqE}\right) \tag{7}$$

Figure 8a shows the fitting parameters for DT junctions in dark using eq 7. The optimum Φ_{FN} decreases about 46% from 3.15 eV at 185 K to 1.70 eV at 300 K at positive bias, while the corresponding decrease is about 14% from 1.75 eV at 185 K to 1.50 eV at 300 K at negative bias, respectively. The barrier height is larger at the positive bias than that at the negative side, which probably resulted from the asymmetric electrode/molecule interfaces as described above. Thus the barrier height is both temperature- and bias-dependent. SAMs of OT, NDT, DDT, and M-1 were systematically simulated to understand molecular length-dependent tunneling (see Figure 8b). The Φ_{FN} of alkanethiols decreases with increasing molecular length from about 3.0 eV for OT down to 2.5 eV for DDT in dark. For the conjugated M-1 molecule, the barrier is about 2.0 eV. The overall results agree well with the Simmons fittings.

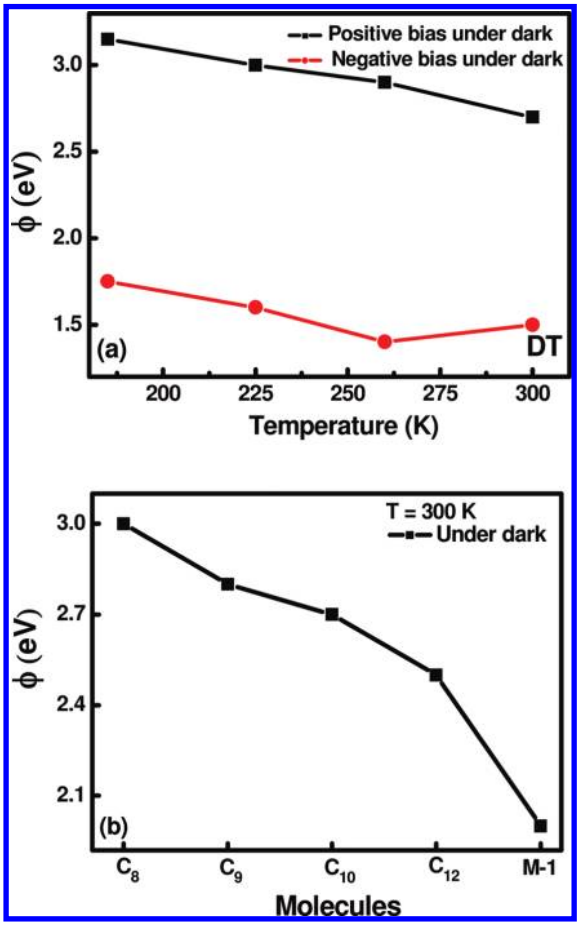

Figure 8. Best-fitting parameters obtained by the Fowler–Nordheim tunneling for (a) the DT junction at different temperatures and (b) different molecules at 300 K both in dark conditions, respectively.

DISCUSSION

The above results confirm the important impacts of the electrode/molecule interface(s),[22] light illumination,[55] temperature, and molecular conformation on the description of the charge transport in SAMs-based molecular junctions.[60] Charge transport across metal–molecule–metal junctions depends strongly on the position of the electrode Fermi levels (E_F) relative to the lowest unoccupied molecular orbital (LUMO) and the highest occupied molecular orbital (HOMO) of the molecular bridge.[61] To understand the effect of asymmetry

dx.doi.org/10.1021/jp300467c | J. Phys. Chem. C 2012, 116, 10986–10994

electrode/molecule interfaces on the position of the Fermi level, simple energy level diagrams of the crossbar junction were given in Figure 9. Once the molecule contacted with the

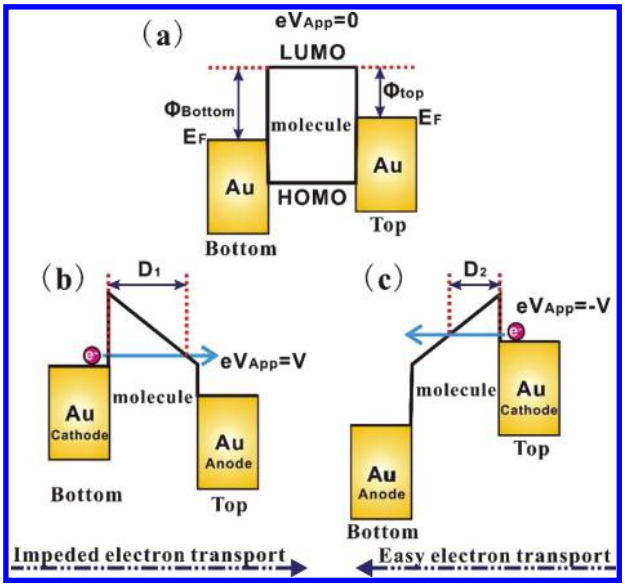

Figure 9. Simple energy level diagrams for the Au-SAMs-Au crossbar junctions, showing the asymmetry electrode/molecule interfaces (a) under zero bias, (b) under positive bias, and (c) under negative bias situations, respectively.

electrodes, the surface dipole layer may induce a shift of the vacuum level, which alters the E_F up or down.[61,62] It is difficult to know exactly the position of E_F within the molecular energy gap. As a first approximation, we assumed a band lineup corresponding to the E_F at the middle of the gap between the HOMO and LUMO.[63,64] According to the above simulations, we supposed the barrier height at the bottom electrode (Φ_{bottom}) is larger than that at the top (Φ_{top}) (see Figure 9a). Figure 9b,c shows diagrams at the positive and negative applied bias conditions, respectively. It is worthwhile to mention that the barrier shape transforms from trapezoidal to triangular at a different bias.[37,38] It is obvious that the barrier height under positive bias is larger than that under the negative side due to the asymmetry Au/molecule interfaces. Therefore, the electron transport in the junction should be easier under negative biases. This assumption could justify the pronounced asymmetry electrode/molecule interface(s) of our stamp-printing crossbar junctions, which agrees with the experimental observations very well.

The optimum fitting parameter Φ is typically considered an effective transport barrier.[49] The "photo" current is higher than the "dark" one at the same voltage (see Figure 3), implying that the effective charge barrier is relatively low under light conditions. Moreover, the light absorption may generate a carrier-contributing photocurrent due to photon-excited electrons into the LUMO.[30,65] Likewise, it is reasonable to assume that the charge carrier mobility and thus the junction conductivity can be enhanced by thermal activation with increase of the substrate temperature.[65] However, previous studies on alkanethiols indicate there are no significant temperature-dependent and thermal activation $I-V$ characteristics.[53,66,67] The temperature dependence in our case may result from the stamp-printing top Au electrode/molecule interface as discussed above. At low temperature, the top SAMs/Au interface is probably just a weak link,[68] and the effective charge barrier is thus relatively large. However the contact may become stronger upon the temperature increase, and the $I-V$ curves exhibited more symmetry, too.

The effect of molecular length on junction charge transport is extensively studied.[49,62,69] It is shown that long-chain alkanethiols are inhibited from standing upright on the electrode surface, while short-chain ones are regarded as the optimized standing-up configuration.[44,69,70] Therefore, the charge barrier decreases with the increase of molecular length, which is in accordance with our results simulated by the Simmons and F–N models. The charge transport in conjugated molecules was more efficient than that through alkanethiols. A possible reason is that the energy barrier height in conjugated molecular junctions should be smaller than that in the alkanethiol ones.[71]

CONCLUSION

In summary, addressable molecular crossbar junctions with different alkanethiol and conjugated SAMs were fabricated using a PDMS stamp-printing method. We systematically studied the charge transport and switching mechanisms of the Au/SAMs/Au crossbar junctions via temperature-dependent $I-V$ measurements and theoretical simulations. The direct tunneling plays a dominant role at low bias (−1 to +1 V) and low temperature (91–185 K) in both dark and light conditions, while the F–N tunneling is only applicable within ±2.5 V in the dark situation at higher temperatures (185–300 K). The charge injection barrier height is dependent on the electrode/molecule interfacial structure, light illumination, substrate temperature, and molecular length/conjugation. In details, (I) the asymmetry Au/SAMs interfaces may induce an asymmetry Au fermi level E_F, and the barrier height is thus larger at the positive bias than at the negative side. (II) Lower barrier height is observed under light illumination because the light absorption may generate carrier contributing photocurrent. (III) The barrier falls off with the increase of temperature owning to the stronger stamp-printing SAMs/Au contact at higher temperature. (IV) The charge barrier decreases with the increase of both molecular length and conjugation degree. All of the above results suggest that the charge transport across the crossbar junctions can be tuned through varying the factors such as light illumination, substrate temperature, and/or molecular length/conjugation. Our work may provide some useful strategies for developing SAMs-based molecular electronic devices.

ASSOCIATED CONTENT

Supporting Information

Representative plots of the $I-V$ temperature dependence based on the hopping conduction, P–F, and thermionic emission models, respectively. Table summarized with the best fitting parameters of α, Φ, and β calculated from the Simmons model for the molecules of OT, NDT, DT, DDT, and M-1, respectively. This material is available free of charge via the Internet at http://pubs.acs.org.

AUTHOR INFORMATION

Corresponding Author

*Phone: 138 0407 5191. Fax: +86-24-8369 0506. E-mail: jcli@mail.neu.edu.cn.

Notes

The authors declare no competing financial interest.

■ ACKNOWLEDGMENTS

Financial support comes from the Specialized Research Fund for the Doctoral Program of Higher Education of China (Grant No. 20100042120023) and the Fundamental Research Funds for Central Universities of China (N110403001).

■ REFERENCES

(1) Lu, Q.; Liu, K.; Zhang, H. M. *ACS Nano* **2009**, *3*, 3861−3868.
(2) Vilan, A. *J. Phys. Chem. C* **2007**, *111*, 4431−4444.
(3) Xu, Y. J.; Fu, X. Z. *Langmuir* **2009**, *25*, 9840−9846.
(4) Shi, J. S.; Chan-Park, M. B.; Li, C. M. *ACS Appl. Mater. Interfaces* **2011**, *3*, 1880−1886.
(5) Heremans, P.; Gelinck, G. H.; Muller, R.; Baeg, K. J.; Kim, D. Y.; Noh, Y. Y. *Chem. Mater.* **2011**, *23*, 341−358.
(6) Son, D. I.; Park, D. H.; Kim, J. B.; Choi, J. W.; Kim, T. W.; Angadi, B.; Yi, Y.; Choi, W. K. *J. Phys. Chem. C* **2011**, *115*, 2341−2348.
(7) Sessolo, M.; Bolink, H. J. *Adv. Mater.* **2011**, *23*, 1829−1845.
(8) Li, Y. N.; Sonar, P.; Singh, S. P.; Soh, M. S.; Meurs, M. V.; Tan, J. *J. Am. Chem. Soc.* **2011**, *133*, 2198−2204.
(9) Shibano, Y.; Imahori, H.; Adachi, C. *J. Phys. Chem. C* **2009**, *113*, 15454−15466.
(10) Karuppiah, K. S. K.; Zhou, Y.; Woo, L. K. *Langmuir* **2009**, *25*, 12114−12119.
(11) Wang, W.; Zhang, S. S.; Chinwangso, P. *J. Phys. Chem. C* **2009**, *113*, 3717−3725.
(12) Kelly, K. F.; Shon, Y. S.; Lee, T. R. *J. Phys. Chem. B* **1999**, *103*, 8639−8642.
(13) Cooper, E.; Leggett, G. J. *Langmuir* **1998**, *14*, 4795−4801.
(14) Yang, G. H.; Qian, Y. L.; Engtrakul, C.; Sita, L. R.; Liu, G. Y. *J. Phys. Chem. B* **2000**, *104*, 9059−9062.
(15) Miao, L.; Seminario, J. M. *J. Chem. Phys.* **2007**, *126*, 184706.
(16) Siram, R. B. K.; Tandy, K.; Horecha, M.; Formanek, P.; Stamm, M.; Gevorgyan, S.; Krebs, F. C.; Kiriy, A.; Meredith, P.; Burn, P. L.; Namdas, E. B.; Patil, S. *J. Phys. Chem. C* **2011**, *115*, 14369−14376.
(17) Frederiksen, T.; Munuera, C.; Ocal, C. *ACS Nano* **2009**, *3*, 2073−2080.
(18) Beebe, J. M.; Kim, B. S.; Frisbie, C. D. *ACS Nano* **2008**, *2*, 827−832.
(19) Liu, H. M.; Wang, N.; Zhao, J. W. *ChemPhysChem* **2008**, *9*, 1416−1424.
(20) Tevis, I. D.; Palmer, L. C.; Herman, D. J.; Murray, I. P.; Stone, D. A.; Stupp, S. I. *J. Am. Chem. Soc.* **2011**, *133*, 16486−16494.
(21) Wang, G.; Kim, T. W.; Jo, G. H. *J. Am. Chem. Soc.* **2009**, *131*, 5980−5985.
(22) Beebe, J. M.; Engelkes, V. B.; Miller, L. L.; Frisbie, C. D. *J. Am. Chem. Soc.* **2002**, *124*, 11268−11269.
(23) Tan, A.; Balachandran, J.; Sadat, S.; Gavini, V.; Dunietz, B. D.; Jang, S. Y.; Reddy, P. *J. Am. Chem. Soc.* **2011**, *133*, 8838−8841.
(24) Yang, W. R.; Jones, M. W.; Li, X. L. *J. Phys. Chem. C* **2008**, *112*, 9072−9080.
(25) Kim, B. S.; Beebe, J. M.; Jun, Y. *J. Am. Chem. Soc.* **2006**, *128*, 4970−4971.
(26) Sharma, G. D.; Balaraju, P.; Sharma, S. K.; Roy, M. S. *Synth. Met.* **2008**, *158*, 620−629.
(27) Lee, T.; Wang, W. Y.; Klemic, J. F. *J. Phys. Chem. B* **2004**, *108*, 8742−8750.
(28) Wang, G.; Kim, T. W.; Jang, Y. H.; Lee, T. *J. Phys. Chem. C* **2008**, *112*, 13010−13016.
(29) Kaun, C. C.; Guo, H. *Nano Lett.* **2003**, *3*, 1521−1525.
(30) Farag, A. A. M.; Yahia, I. S.; Wojtowicz, T.; Karczewski, G. *J. Phys. Appl. Phys.* **2010**, *1088*, 0022−3727.
(31) Li, J. C. *Chem. Phys. Lett.* **2009**, *473*, 189−192.
(32) Jiang, P.; Morales, G. M.; You, W.; Yu, L. P. *Chem. Int. Ed.* **2004**, *43*, 4471−4475.
(33) Morales, G. M.; Jiang, P.; Yuan, S. W.; Lee, Y. G.; Sanchez, A.; You, W.; Yu, L. P. *J. Am. Chem. Soc.* **2005**, *127*, 10456−10457.
(34) Ruibal, M.; Ferro, G.; Blanch, M.; Veira, J. A.; Maza, J.; Vidal, F. *Physica C* **2007**, *460*, 819−820.
(35) Shadnam, M. R.; Kirkwood, S. E.; Fedosejevs, R.; Amirfazli, A. *J. Phys. Chem. B* **2005**, *109*, 11996−12002.
(36) Junginger, F.; Klaui, M.; Backes, D.; Rudiger, U.; Kasama, T.; Dunin-Borkowski, R. E.; Heyderman, L. J.; Vaz, C. A. F.; Bland, J. A. C. *Appl. Phys. Lett.* **2007**, *90*, 132506.
(37) Pakoulev, A. V.; Burtman, V. *J. Phys. Chem. C* **2009**, *113*, 21413−21421.
(38) Beebe, J. M.; Kim, B.; Gadzuk, J. W.; Frisbie, C. D.; Kushmerick, J. G. *Phys. Rev. Lett.* **2006**, *97*, 026801.
(39) Hutchison, G. R.; Ratner, M. A.; Marks, T. J. *J. Am. Chem. Soc.* **2005**, *127*, 16866−16881.
(40) Chen, J.; Calvet, L. C.; Reed, M. A.; Carr, D. W.; Grubisha, D. S.; Bennett, D. W. *Chem. Phys. Lett.* **1999**, *313*, 741−748.
(41) DiBenedetto, S. A.; Facchetti, A.; Ratner, M. A.; Marks, T. J. *J. Am. Chem. Soc.* **2009**, *131*, 7158−7168.
(42) Beebe, J. M.; Engelkes, V. B.; Liu, J. Q. *J. Phys. Chem. B* **2005**, *109*, 5207−5215.
(43) Lee, T.; Wang, W. Y.; Reed, M. A. *Ann. N.Y. Acad. Sci.* **2003**, *1006*, 21−35.
(44) Huang, Q. L.; Li, J. F.; Evmenenko, G. A. *Chem. Mater.* **2006**, *18*, 2431−2442.
(45) Huang, Q. L.; Evmenenko, G.; Dutta, P. *J. Am. Chem. Soc.* **2003**, *125*, 14704−14705.
(46) Kitagawa, K.; Morita, T.; Kimura, S. *J. Phys. Chem. B* **2005**, *109*, 13906−13911.
(47) Li, X. L.; He, J.; Hihath, J. *J. Am. Chem. Soc.* **2006**, *128*, 2135−2141.
(48) Seo, K.; Lee, H. *ACS Nano* **2009**, *3*, 2469−2476.
(49) Chu, C. W.; Na, J. S.; Parsons, G. N. *J. Am. Chem. Soc.* **2007**, *129*, 2287−2296.
(50) Seminario, J. M.; Cecilia, E.; Derosa, P. A. *J. Am. Chem. Soc.* **2001**, *123*, 5616−5617.
(51) Sharma, G. D.; Balaraju, P.; Sharma, S. K.; Roy, M. S. *Synth. Met.* **2008**, *158*, 620−629.
(52) Fan, F. F.; Yao, Y. X.; Cai, L. T.; Cheng, L.; Tour, J. M.; Bard, A. J. *J. Am. Chem. Soc.* **2004**, *126*, 4035−4042.
(53) Wang, W. Y.; Lee, T.; Reed, M. A. *J. Phys. Chem. B* **2004**, *108*, 18398−18407.
(54) Hanss, D.; Walther, M. E.; Wenger, O. S. *Coord. Chem. Rev.* **2010**, *254*, 2584−2592.
(55) Zhou, J. F.; Xu, B. Q. *Appl. Phys. Lett.* **2011**, *99*, 042104.
(56) Holmlin, R. E.; Haag, R.; Chabinyc, M. L. *J. Am. Chem. Soc.* **2001**, *123*, 5075−5085.
(57) Wold, D. J.; Frisbie, C. D. *J. Am. Chem. Soc.* **2001**, *123*, 5549−5556.
(58) Pananakakis, G.; Ghibaudo, G.; Kies, R.; Papadas, C. *J. Appl. Phys.* **1995**, *78*, 2635−2641.
(59) Agarwal, A. K.; Seshadri, S.; Rowland, L. B. *IEEE Electron Device Lett.* **1997**, *18*, 592−594.
(60) O'Mullane, A. P.; Fay, N.; Nafady, A.; Bond, A. M. *J. Am. Chem. Soc.* **2007**, *129*, 2066−2073.
(61) Fan, F. R. F.; Yang, J. P.; Cai, L. T.; Price, D. W.; Dirk, S. M.; Kosynkin, D. V.; Yao, Y. X.; Rawlett, A. M.; Tour, J. M.; Bard, A. J. *J. Am. Chem. Soc.* **2002**, *124*, 5550−5560.
(62) Tan, A.; Balachandran, J.; Sadat, S.; Gavini, V.; Dunietz, B. D.; Jang, S. Y.; Reddy, P. *J. Am. Chem. Soc.* **2011**, *133*, 8838−8841.
(63) Subramanian, V.; Wolf, E. E.; Kamat, P. V. *J. Am. Chem. Soc.* **2004**, *126*, 4943−4950.
(64) Jakob, M.; Levanon, H.; Kamat, P. V. *Nano Lett.* **2003**, *3*, 353−358.
(65) Chirvase, D.; Chiguvare, Z.; Knipper, M.; Parisi, J.; Dyakonov, V.; Hummelen, J. C. *J. Appl. Phys.* **2003**, *93*, 3376−3383.
(66) O'Brien, B.; Sahalov, H.; Searson, P. C. *Appl. Phys. Lett.* **2010**, *97*, 043110.

(67) Duda, J. C.; Saltonstall, C. B.; Norris, P. M.; Hopkins, P. E. *J. Chem. Phys.* **2011**, *134*, 094704.
(68) Gonzalez, C.; Mujica, V.; Ratner, M. A. *Mol. Electron. II* **2002**, *960*, 163−176.
(69) Millone, M. A. D.; Hamoudi, H.; Rodriguez, L.; Rubert, A.; Benitez, G. A.; Vela, M. E.; Salvarezza, R. C.; Gayone, J. E.; Sanchez, E. A.; Grizzi, O.; Dablemont, C.; Esaulov, V. A. *Langmuir* **2009**, *25*, 12945−12953.
(70) Hines, T.; Diez-Perez, I.; Hihath, J.; Liu, H. M.; Wang, Z. S.; Zhao, J. W.; Zhou, G.; Muellen, K.; Tao, N. J. *J. Am. Chem. Soc.* **2010**, *132*, 11658−11664.
(71) Cygan, M. T.; Dunbar, T. D.; Arnold, J. J.; Bumm, L. A.; Shedlock, N. F.; Burgin, T. P.; Jones, L.; Allara, D. L.; Tour, J. M.; Weiss, P. S. *J. Am. Chem. Soc.* **1998**, *120*, 2721−2732.
(72) Ditzler, L. R.; Karunatilaka, C.; Donuru, V. R. *J. Phys. Chem. C* **2010**, *114*, 4429−4435.